On the evolution of film roughness during magnetron sputtering deposition

Turkin, A. A. ; Pei, Y. T.; Shaha, K. P.; Chen, C. Q.; Vainchtein, D. I.; de Hosson, J. Th. M.

Published in:
Journal of Applied Physics

DOI:
10.1063/1.3506681

Publication date:
2010

On the evolution of film roughness during magnetron sputtering deposition

A. A. Turkin,[1,2] Y. T. Pei,[1] K. P. Shaha,[1] C. Q. Chen,[1] D. I. Vainshtein,[1] and J. Th. M. De Hosson[1,a)]
[1]*Department of Applied Physics, Materials Innovation Institute M2i and Zernike Institute for Advanced Materials, University of Groningen, Nijenborgh 4, 9747 AG Groningen, The Netherlands*
[2]*National Science Center, Kharkov Institute of Physics & Technology, 1 Akademicheskaya Str., UA-61108 Kharkov, Ukraine*

(Received 5 September 2010; accepted 27 September 2010; published online 15 November 2010)

The effect of long-range screening on the surface morphology of thin films grown with pulsed-dc (p-dc) magnetron sputtering is studied. The surface evolution is described by a stochastic diffusion equation that includes the nonlocal shadowing effects in three spatial dimensions. The diffusional relaxation and the angular distribution of the incident particle flux strongly influence the transition to the shadowing growth regime. In the magnetron sputtering deposition the shadowing effect is essential because of the configuration of the magnetron system (finite size of sputtered targets, rotating sample holder, etc.). A realistic angular distribution of depositing particles is constructed by taking into account the cylindrical magnetron geometry. Simulation results are compared with the experimental data of surface roughness evolution during 100 and 350 kHz p-dc deposition, respectively. © *2010 American Institute of Physics*. [doi:10.1063/1.3506681]

I. INTRODUCTION

Surface roughness affects the performance of thin solid films and films. Over the last decade considerable efforts have been devoted to investigations of surface roughness evolution during deposition of thin films (for a review see Refs. 1–7). The roughness is caused by irregular and stochastic precipitation of depositing particles due to the fluctuation of particle flux (noise) and shadowing effects. Without subsequent lateral transport, this irregular precipitation results inevitably in a profile of rapidly advancing roughness. Therefore, to improve the performance of thin solid films, i.e., to reduce roughness, several deposition techniques[8–10] use concurrent impingements by energetic ions to increase the diffusion mobility of surface atoms. In our investigations of film deposition with various compositions we use a closed-field unbalanced magnetron sputtering system (Teer UDP 400/4).[11,12] The advantage of this system is that the argon plasma can be used for both the sputtering of targets of different precursor materials and the concurrent ion impingement of the growing film. The microstructural properties of nanocomposite films based on diamond-like carbon can be controlled effectively in the regime of pulsed-dc (p-dc) sputtering.[11] Ion mass/energy spectrometry of the plasma has shown that by changing waveform, frequency, width of dc pulses the flux, and the energy distribution of Ar^+ ions to the growing films can be changed over a very broad range. As a result the surface morphology of the films evolves from cauliflowerlike patterns to shallow domes at 100 kHz, weak ripples at 250 kHz and flat surface with nanometer-sized bumps at 350 kHz.[11]

In our previous work,[13] we have presented an analysis of smoothing mechanism of the film grown with p-dc magnetron sputtering. Roughness evolution was described by a model based on a linear stochastic differential equation with the second- and fourth-order gradient relaxation terms, which accounts for diffusion along the film surface. The second-order term was attributed to the downhill flow resulting from the continuous bombardment of the growing film by Ar^+ ions. The fourth-order term was associated with the surface diffusion of adatoms driven by the gradient of the chemical potential along the surface. This model belongs to a class of local models, in which the film growth rate depends on the local properties of the surface. A general feature of these models is that growth rate of the film at a given point depends only on film thickness and its derivatives at that particular point. In local models the incoming particle flux is directed perpendicular to the substrate; and the film roughness is caused only by the deposition noise, i.e., by spatial-temporal fluctuations originating from the particle source.

In our experiments with p-dc magnetron sputtering, we studied the transition from the roughening regime to the smoothing one. We have found that the roughness developed during 100 kHz p-dc deposition was smoothed out rapidly by the subsequent 350 kHz deposition. The time dependence of the root mean square (rms) roughness of films deposited at 100 kHz p-dc is essentially linear:[14] $w(t) \sim t^{\beta}$ with $\beta \sim 1$, where β is the growth exponent. In local models of random deposition the largest growth exponent $\beta = 1/2$ is attained at zero mobility of atoms along the surface.[15] This implies that some other roughening mechanism besides noise is present during deposition with p-dc magnetron sputtering. The fast growth of roughness can be attributed to geometrical shadowing, the process in which some parts of the surface are shadowed from the incoming flux by other parts of the growing surface.[16–24] Initially, the smooth surface roughens due to the noise. If the depositing particles strike the substrate from a broad range of angles, the shadowing effect sooner or later becomes important. Peaks of the surface undulation are exposed to incoming particles from all directions and thus grow

a)Electronic mail: j.t.m.de.hosson@rug.nl.

faster than the average growth rate. At the same time, valleys of the surface undulation receive fewer particles since they are screened by peaks; therefore, their growth lags behind. This leads to instability of the planar surface and results in the development of a mountain landscape or columnar structure, i.e., the film becomes extremely rough if the surface mobility of atoms is too low.

The objective of this paper is to incorporate shadowing effects in three spatial dimensions by taking into account the angular distribution of depositing particles and to revise accordingly our model.[13] The main purpose is to demonstrate the important role of angular distribution of depositing particles that is inevitably connected to the motion of substrates passing by one magnetron to another. We also investigate the influence of diffusion parameters on the evolution of surface morphology.

The necessary prerequisite of the shadowing effect is the angular distribution of the incident particle flux. In the magnetron sputtering system, the shadowing effect must be essential, because the flux of depositing particles has an angular distribution due to the structure of the magnetron installation (finite size of sputtering targets, rotation of sample holder in a cylindrical configuration or linear motion in a planar arrangement of magnetrons, etc.). As an example, we simulate the film growth with a realistic angular distribution of depositing particles, which has been constructed by taking into account the cylindrical configuration of magnetrons. Simulation results are in good agreement with the experimental data on 100 and 350 kHz p-dc deposition.

II. MODEL OF SHADOWING GROWTH

Because of computational difficulties most of pioneering simulation studies have been performed in two dimensions.[16–22] To our knowledge, Yao and Guo[23] were the first who solved numerically the continuum equation with the second-order diffusion term to describe shadowing growth in three dimensions. Using the concept of the exposure angle,[16,17] according to which the local growth rate at a point is roughly proportional to the exposure angle of this point, Yao and Guo[23] have proposed a continuum equation for shadowing growth

$$\frac{\partial h(\mathbf{r},t)}{\partial t} = G\omega(\mathbf{r},\{h\}) + D_2\nabla^2 h(\mathbf{r},t) + \eta(\mathbf{r},t), \tag{1}$$

where $h(\mathbf{r},t)$ is the film thickness. The second term in the right-hand side is the Edwards–Wilkinson diffusion term.[25] The stochastic noise term $\eta(\mathbf{r},t)$ is related to the fluctuations of deposition flux and is assumed to be Gaussian and uncorrelated with zero mean. The noise covariance is given by

$$\langle \eta(\mathbf{r},t)\,\eta(\mathbf{r}',t')\rangle = D\,\delta(\mathbf{r}-\mathbf{r}')\,\delta(t-t'), \tag{2}$$

where $\langle \ldots \rangle$ stands for the ensemble average, D is the deposition noise strength, $\delta(\mathbf{r}-\mathbf{r}')=\delta(x-x')\,\delta(y-y')$ is the two-dimensional (2D) delta-function.

The first term is the growth rate at location $\mathbf{r}$ of the growing surface, where G is the mean growth rate of the film, $\omega(\mathbf{r},\{h\})$ is the normalized exposure solid angle at location $\mathbf{r}$ in the form[23]

$$\omega(\mathbf{r},\{h\}) = \frac{\Omega(\mathbf{r},\{h\})}{\bar{\Omega}}, \tag{3}$$

where $\Omega(\mathbf{r},\{h\})$ is the exposure solid angle and $\bar{\Omega}$ is the mean exposure solid angle. The exposure solid angle depends on the surface profile around the point $\mathbf{r}$

$$\Omega(\mathbf{r},\{h\}) = \int_0^{2\pi} d\varphi \int_0^{\theta(\varphi)} d\theta' \sin\,\theta', \tag{4}$$

where θ is the polar angle and φ is the azimuthal angle in the local spherical coordinates with the origin at the surface point $\mathbf{r}$. $\theta(\varphi)$ defines the maximum angle of a line of sight access to the surface point $\mathbf{r}$.

The first term in Eq. (1) represents a simple way to demonstrate the shadowing effect. Using Eq. (1) Yao and Guo[23] performed numerical calculations on a 96×96 lattice, which have shown that the surface width increases linearly with time after some transient period. Later on small-scale three-dimensional (3D) numerical calculations of the continuum equation of shadowing with lateral growth confirmed the result of Yao and Guo.[24,26]

We have tried to apply the approach of Ref. 23 to explain our results on linear growth of the film roughness[14] but our simulation has shown that the film roughness increases too fast as compared to experimental observations. The reason is that in the approach of Yao and Guo the depositing particles move toward the surface at random incident angles. In fact, they used the uniform angular distribution of directions of incoming particles

$$P(\theta,\varphi) = \frac{1}{2\pi}, \quad \int_0^{2\pi} d\varphi \int_0^{\pi/2} P(\theta,\varphi)\sin\,\theta d\theta = 1. \tag{5}$$

In this case the fraction of particles depositing at oblique angles is very high. These particles induce a very strong shadow effect resulting in a fast growth of rms roughness.

In this paper, we propose a 3D continuum model (see our previous work[13]) with the additional term, which takes into account the angular distribution of depositing particles

$$\frac{\partial h(\mathbf{r},t)}{\partial t} = F(\mathbf{r},\{h\}) + D_2\nabla^2 h(\mathbf{r},t) - D_4\nabla^2[\nabla^2 h(\mathbf{r},t)] + \eta(\mathbf{r},t), \tag{6}$$

$$F(\mathbf{r},\{h\}) = \int_0^{2\pi} d\varphi \int_0^{\theta(\varphi)} f(\theta',\varphi)\sin\,\theta'\,d\theta', \tag{7}$$

where $f(\theta,\varphi)$ is the angular distribution of depositing particles, integration is carried out over the exposure solid angle $\Omega(\mathbf{r},\{h\})$ at a point $\mathbf{r}$ (Fig. 1). D_2 and D_4 are the positive diffusivity parameters that control the atomic mobility along the surface. The Edwards–Wilkinson diffusion coefficient D_2 is related to ballistic effects due to ion bombardment resulting in downhill diffusion along the inclined surface.[27] We believe that in the case of p-dc magnetron sputtering deposition the Edwards–Wilkinson diffusion is due to the flux of energetic Ar^+ ions to the growing film. Following Mullins,[28] the kinetic coefficient D_4 is usually attributed to the surface diffusion of adatoms driven by the gradient of the chemical

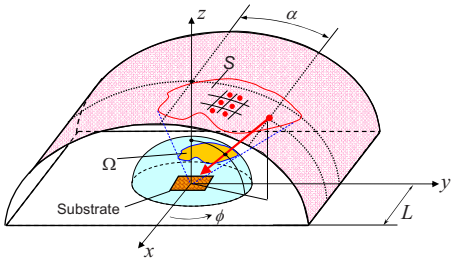

FIG. 1. (Color online) System geometry used in modeling the flux of atoms onto a planar substrate. Real discrete targets in the magnetron installation are replaced with the continuous cylindrical surface that emits atoms. Label *S* denotes the area that is seen from a given position on the growing film, i.e., which lies within the solid angle Ω.

potential along the surface, which is associated with the gradient of the local curvature. According to numerical examination of Eq. (6) without shadowing, the coefficient D_4 controls the smoothing process of high-frequency or small-scale undulations[29] (see also the experimental study of simultaneous short-range smoothing and global roughening[30]). The important feature of the growth Eq. (6) is that shadowing, noise and relaxation are assumed to contribute additively to the roughness evolution. In a real situation other effects can be present. For example the diffusion coefficient D_2 may depend on position on the film surface because of possible influence on the ion flux of a higher electrical field in the vicinity of the surface protrusions with a high curvature.

It should be noted that there exists a nonlocal smoothing mechanism in addition to diffusion along the surface. Depending on deposition conditions, particles can either stick to or bounce off from their impact points depending on a sticking coefficient. Nonsticking particles are reflected diffusely (or re-emitted) and can arrive at other surface points including shadowed valleys.[24] Monte Carlo simulations have shown that at small sticking coefficients this type of relaxation is stronger than the roughening effects of shadowing; and Monte Carlo simulations produced smooth surfaces with small β values.[31] At sticking coefficients close to unity, the shadowing effect becomes the dominant process and columnar rough morphologies start to form.[31]

To avoid computational difficulties in Eq. (7), we neglected the reflection of depositing particles from the film surface.

To analyze the growth equation it is convenient to introduce dimensionless variables

$$(u,v,z) = \frac{(x,y,h)}{l_0}, \quad \tau = t/\tau_0, \tag{8}$$

where the length scale l_0 and time scale τ_0 can be defined as

$$l_0 = D_2/G, \quad \tau_0 = l_0/G. \tag{9}$$

The growth equation in dimensionless variables is given by

$$\frac{\partial z}{\partial \tau} = \frac{F(u,v)}{G} + \nabla^2 z - d_4 \nabla^2(\nabla^2 z) + \chi(u,v,\tau),$$

$$\langle \chi(u,v,\tau)\chi(u',v',\tau')\rangle = d\,\delta(u-u')\,\delta(v-v')\,\delta(\tau-\tau'),$$

$$d = \frac{DG^2}{D_2^3}, \quad d_4 = \frac{D_4 G^2}{D_2^3}. \tag{10}$$

The important parameter of the model [Eq. (10)] is the dimensionless noise strength d. The following reasoning shows the relation of this parameter to the real deposition conditions. The deposition noise strength is proportional to the mean atomic flux,[1,13,32] the diffusion coefficient D_2 depends on the flux of Ar+ ions bombarding the growing film.[13] Therefore, the dimensionless deposition noise strength can be represented schematically as a power of the ratio of atomic flux to Ar^+ flux

$$d = \frac{DG^2}{D_2^3} \propto \frac{G^3}{D_2^3} \propto \left(\frac{\text{Atomic flux}}{\text{Ar}^+ \text{ flux}}\right)^3. \tag{11}$$

At a high value of d one can expect fast development of noise-driven roughness of initially flat substrate and then a transition to the shadow instability. Therefore, the incubation time (or the critical film thickness) depends on the parameter d. In Sec. III, we present typical results on shadowing growth and demonstrate the influence of diffusion parameters on the evolution of surface morphology.

III. RESULTS OF MODELING APPROACH

Equation (6) was solved numerically with the Euler algorithm in time. Spatial derivatives are approximated by finite differences on a discrete 2D mesh with N×N points (N=128, 256, and 512, respectively)

$$h_{n,m}^{\alpha+1} = h_{n,m}^{\alpha} + \Delta t F_{n,m} + \sqrt{\frac{D\Delta t}{\Delta x^2}}\xi_{nm}^{\alpha} + \Delta t \frac{D_2}{\Delta x^2}(h_{n+1,m}^{\alpha} + h_{n-1,m}^{\alpha} + h_{n,m+1}^{\alpha} + h_{n,m-1}^{\alpha} - 4h_{n,m}^{\alpha}) + \Delta t \frac{D_4}{\Delta x^4}(\ldots 13 \text{ terms}\ldots). \tag{12}$$

The time step Δt and the mesh size Δx were selected according to the stability criterion

$$\frac{4\Delta t D_2}{\Delta x^2} + \frac{32\Delta t D_4}{\Delta x^4} < 1. \tag{13}$$

The discrete deposition noise is generated in each time step t_α; the random numbers ξ_{nm}^{α} are taken from the Gaussian distribution with mean zero and unit variance. To find the flux of depositing atoms the solid angles Ω_{nm} are calculated in all mesh point using local spatial spherical coordinates. For each mesh point the azimuthal angle is discretized into slices, and the polar angle θ is computed for each of these slices. Optimal calculation speed and result reproducibility was obtained at number of slices equals 72. Equation (7) is used with a selected angular distribution function in order to find the flux in each point of the surface.

The symmetric boundary conditions are used, i.e., the simulated profile $h(\mathbf{r},t)$ is mirror imaged at the boundaries, $x=0$, $x=x_N$, $y=0$, and $y=y_N$ to prevent the diffusion of atoms from the simulation area and to calculate the deposition flux at the periphery of the simulation area. This type of boundary conditions is appropriate for modeling of deposition onto initially rough surfaces.

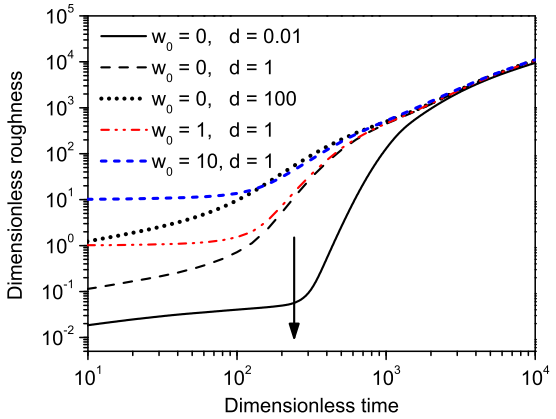

FIG. 2. (Color online) Numerical solution to Eqs. (10) and (14) with the uniform angular distribution of deposition flux Eq. (5). Dimensionless variables are defined by Eqs. (8) and (9), and w_0 is the initial roughness of substrate or interlayer. The sample size is 128×128, $\Delta x=1$, and $D_4=0$.

Simulations have shown that in the regime of shadowing growth the mean growth rate decreases with time. The reason is that valleys deepen progressively and result in the decrease in exposure solid angles therein. This means that on average the upper integration limit $\theta(\varphi)$ in Eq. (7) decreases, i.e., the mean particle flux to the surface decreases. It should be noted that at this stage of film growth (when the mean local slope greater than unity) the underlying diffusion equation is valid only qualitatively. However, to compare our model with the results of Yao and Guo's work,[23] we have simulated film growth with normalization similar to Eq. (3)

$$\frac{F(\mathbf{r},\{h\})}{G} \to \frac{F(\mathbf{r},\{h\})}{\bar{F}(\mathbf{r},\{h\})}. \tag{14}$$

This normalization has been used by Yao and Guo[23] to ensure that the total incoming particle flux is constant throughout the growth process.

Below, we present simulation results that demonstrate the sensitivity of the model to the variation in the physical parameters. Figure 2 shows the time dependence of rms roughness calculated for different values of dimensionless noise d and initial roughness. The angular distribution of depositing particles was assumed to be independent of angles, i.e., $f(\theta,\varphi)=$const. It is seen that after initial transient period indicated by the arrow in the figure all curves exhibit universal asymptotic behavior of shadowing growth. The duration of the dimensionless transient period is about the same for all curves

$$t^* = \alpha\tau_0 = \alpha\frac{D_2}{G^2}, \quad a \sim 10^2. \tag{15}$$

Therefore, shadowing growth dominates when the film thickness is larger than the critical thickness of the film

$$h^* = \alpha\frac{D_2}{G} \sim \alpha d^{-1/3} \propto \frac{\mathrm{Ar}^+ \text{ flux}}{\text{Atomic flux}}. \tag{16}$$

This result qualitatively agrees with experimental observations, according to which the necessary condition for growth of smooth films is the ion bombardment of enough intensity.

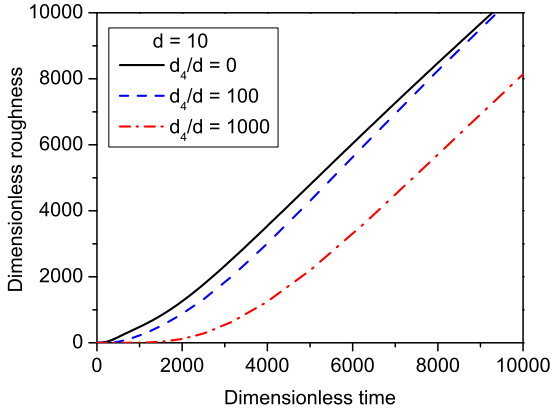

FIG. 3. (Color online) Influence of D_4 on the development of shadowing instability. Numerical solution to Eqs. (10) and (14) with the uniform angular distribution of deposition flux. Dimensionless variables are defined by Eqs. (8) and (9). The sample size 128×128 and $\Delta x=1$.

Figures 3 and 4 show the influence of the parameter D_4 on the film growth. It is seen that the additional relaxation mechanism results in an increase in the transient period (Fig. 3). After the transient period the rms roughness increases linearly with time. It is known that during shadowing growth the surface structure coarsen with time.[19,23] As can be seen from Fig. 4 the diffusion parameter D_4 influences the coarsening behavior. It can be explained as follows. When deposition starts from the smooth substrate, the deposition noise causes the appearance of roughness at atomic level, which provides nuclei for the shadowing growth. Diffusion relaxation destroys these nuclei. The curvature-driven diffusion controlled by the parameter D_4 is especially efficient for such local features.

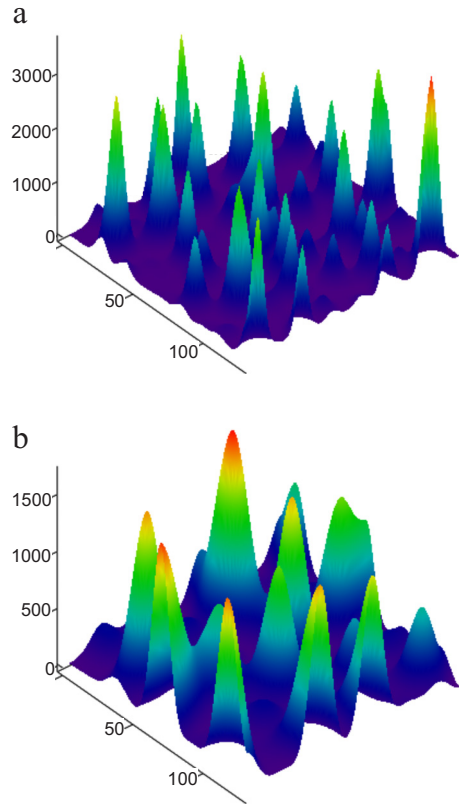

FIG. 4. (Color online) Influence of D_4 on coarsening of surface features at $d=10$. For calculation details see Fig. 3. (a) $d_4/d=0$ and (b) $d_4/d=103$.

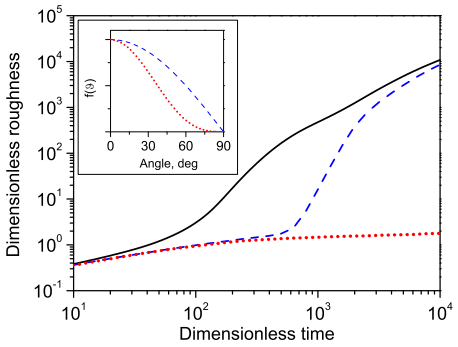

FIG. 5. (Color online) Influence of the angular distribution of depositing flux on the development of shadowing instability. Numerical solution to Eqs. (10) and (14) with the angular distribution of deposition flux $f(\theta,\varphi) \propto \cos^n(\theta)$. The solid line correspond to $n=0$, the dashed and dotted lines correspond to $n=1$ and 3, respectively (corresponding distributions are shown in the inset). Dimensionless variables are defined by Eqs. (8) and (9). The sample size is 128×128, $\Delta x=1$, and $d=10$.

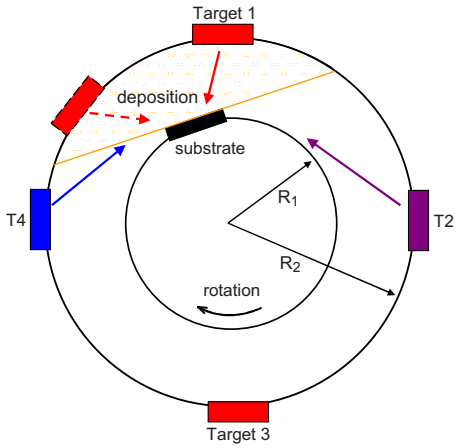

FIG. 6. (Color online) Configuration of the used magnetron sputtering system. The substrate receives sputtered atoms from the region labeled as "deposition."

In Fig. 5, we compare the time dependence of the rms roughness of a film obtained with the angular distribution $f(\theta,\varphi) \propto \cos^n(\theta)$, where $n=0,1,3$. It is seen that for the $\cos^3(\theta)$ distribution the rms roughness evolve very slow. For this type of distribution the fraction of particles with polar angles close to $\theta=90°$ is small compared to the uniform distribution [Eq. (5)]. In practice, a collimation of the sputtered particles is an efficient way to reduce the fraction of particles depositing at oblique angles and to suppress the surface roughness.[33] However, collimation cannot be used for deposition on a substrate of a complicated shape.

IV. COMPARISON WITH EXPERIMENTS

In a real installation, the flux of depositing particles exhibits an angular dependence, which is determined by the geometry of the sputtering chamber, collision, and scattering of particles in the plasma depending on the working pressure, rotation/motion of targets/substrates, etc. The working gas tends to randomize directions from which particles approach the substrate. The assumption of uniform angular distribution is appropriate only for high gas pressure, when the Knudsen number—the ratio of the mean-free path of particles to the characteristic length (sample size or distance between target and sample)—is small. Our deposition installation is typically operating at pressures about 2×10^{-3} mbar. At this pressure, the estimated mean-free path for the sputtered atoms exceeds the target-to-sample distance of 6 to 8 cm. The incoming atoms can thus be assumed to move ballistically. The angular distribution $Y(\beta)$ of atoms emitted from the surface of the target due to normally incident ions is usually assumed to follow a cosinelike distribution $Y(\beta) \propto \cos^n \beta$, where β is the ejection angle of the sputtered atoms with respect to the surface normal.[34,35] The following formula can also represent an angular distribution for normal incidence of ions[36,37]

$$Y(\beta) \propto (1 + B\cos^2\beta)\cos\beta, \tag{17}$$

where B is a fitting parameter. However, because of a special magnetic field configuration in the magnetron installation the deep racetracks form on targets. Therefore, the sputtering yield can be strongly "over-cosine" $Y(\beta) \propto \cos^n \beta$ with $n>1$. The overall effect of the installation geometry and the sputtering details is that the sputtered atoms have an anisotropic distribution of directions, specific to a particular deposition installation. In some cases due to system symmetry the angular distribution of depositing particles can be evaluated analytically.

A. Angular distribution of depositing particles

Schematically, our deposition installation consists of several targets emitting atoms that are depositing onto the substrates mounted on a rotating carousel (Fig. 6), which is comparable to the sputtering process under a planar configuration of multiple magnetrons facing to the substrates mounted on a transport belt as commonly used in coating glass sheets of large dimensions. To find the angular dependence of the atomic flux to the substrate we use the following simplifications (Fig. 6).

- The frame of reference is fixed to the substrate, then the targets rotates around the substrate.
- The rotating targets are approximated by a cylindrical surface emitting particles.

Particles emitted from the cylindrical surface are assumed to follow a linear path to the substrate. The flux of particles depositing to the point (x_0,y_0) on the substrate is the sum of contributions of all surface elements $dS = R_2 d\alpha dx$.

$$F(x_0,y_0) = R_2 \int_{S(x_0,y_0)} \frac{Y[\beta(\alpha,x)]}{[r(\alpha,x)]^2} d\alpha dx, \tag{18}$$

where R_2 is the radius of cylindrical chamber on which the targets are installed (see Fig. 6), α and x are the coordinates on the cylindrical surface, $r(\alpha,x)$ is the distance from the source point to the point on the substrate, $Y(\beta)$ is the angular emission distribution of sputtered particles, and $\beta(\alpha,x)$ is the angle between the local normal and direction to the target (Fig. 7). Note that the flux decreases as the square of the distance away from the source

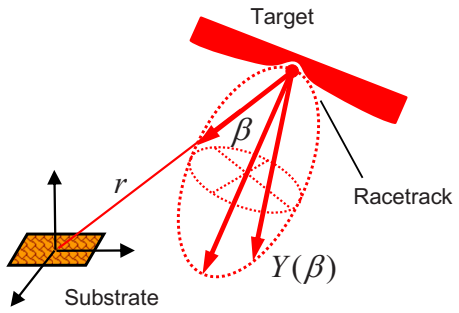

FIG. 7. (Color online) Angular emission distribution of sputtered atoms. The target with the racetrack is shown schematically. Experimentally a deep racetrack is observed on the target. Therefore, it is assumed that atoms are mostly emitted from the racetrack with the over-cosine sputtering yield $Y(\beta) \propto \cos^n \beta$, $n > 1$ [see Eq. (20)].

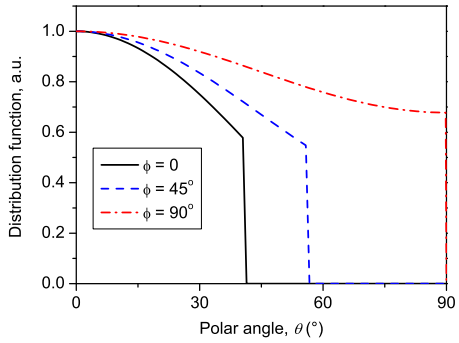

FIG. 8. (Color online) The dependence of distribution on polar angle plotted for several values of azimuthal angle. The sputtering yield $Y(\beta) \propto \cos^3 \beta$. Geometrical parameters are listed in Table I. $\phi = 0$ corresponds to the cross-section y=0 (see Fig. 1).

The angular emission distribution of sputtered particles, i.e., the sputtering yield $Y(\beta)$ from a particular point on the target depends on the energy and angular distribution of Ar^+ flux to the target

$$Y(\beta) = \int y(\beta, \phi, \{E, \theta', \phi'\}) \Phi_{\mathrm{Ar}}(E, \theta', \phi') \sin\theta' d\theta' d\phi dE, \tag{19}$$

where $y(\beta, \phi, \{E, \theta', \phi'\})$ is the average sputtering yield due to an Ar^+-ion with energy E and travel direction defined by θ', ϕ' (spherical coordinates related to the target), $\Phi_{\mathrm{Ar}}(E, \theta', \phi')$ is the distribution of Ar^+ flux at the target. In the following we will use a simple cosinelike emission distribution, that agrees with the Sigmund approximation of linear cascade sputtering[34,38] and experimental data on sputtering of various polycrystalline targets[35,39]

$$Y(\beta) = A \cos^n \beta \quad 1 \leq n. \tag{20}$$

The normalization constant A is related to the mean growth rate G of a smooth film by the relation

$$G = AR_2 \int_{-L}^{L} \int_{0}^{\alpha_{\max}} \frac{\cos^n(\beta)}{r^2} d\alpha dx,$$

where the integration is carried out over the whole area that emits particles.

To find the angular distribution of depositing particles we need to map the "sky" seen from a substrate point (x_0, y_0) to the exposure solid angle $S(x_0, y_0) \rightarrow \Omega(x_0, y_0)$, i.e., to transform the coordinates in the "cylindrical sky" into local spherical coordinates $(\alpha, x) \rightarrow [r(\theta, \phi), \theta, \phi]$. Then Eq. (18) transforms into

$$F(x_0, y_0) = R_2 \int_{\Omega(x_0, y_0)} \frac{Y[\beta(\theta, \phi)]}{[r(\theta, \phi)]^2} \frac{\partial(\alpha, x)}{\partial(\theta, \phi)} d\theta d\phi, \tag{21}$$

where the Jacobian determinant is given by

$$\frac{\partial(\alpha, x)}{\partial(\theta, \phi)} = \det \begin{pmatrix} \frac{\partial \alpha(\theta, \phi)}{\partial \theta} & \frac{\partial \alpha(\theta, \phi)}{\partial \phi} \\ \frac{\partial x(\theta, \phi)}{\partial \theta} & \frac{\partial x(\theta, \phi)}{\partial \phi} \end{pmatrix}$$

$$= \frac{r \sin\theta}{\sqrt{R_2^2 - r^2 \sin^2\theta \sin^2\phi}} \frac{d}{d\theta}(r \sin\theta), \tag{22}$$

where $r(\theta, \phi)$ is the distance from substrate to the point particle source on the cylindrical surface

$$r(\theta, \phi) = \frac{\sqrt{R_2^2 \cos^2\theta + (R_2^2 - R_1^2)\sin^2\theta \sin^2\phi} - R_1 \cos\theta}{\cos^2\theta + \sin^2\theta \sin^2\phi}. \tag{23}$$

Comparison of Eq. (7) with Eq. (21) shows that the angular distribution of depositing particles is given by

$$f(\theta, \phi) = R_2 \frac{Y[\beta(\theta, \phi)]}{[r(\theta, \phi)]^2 \sin\theta} \frac{\partial(\alpha, x)}{\partial(\theta, \phi)}. \tag{24}$$

After some algebra, we find the final expression for the angular distribution of depositing particles

$$f(\theta, \phi) = \begin{cases} \frac{Y(\beta)}{\cos\beta} & \\ 0 & \text{if } \theta > \theta_{\max}(\phi) \end{cases}, \tag{25}$$

where $\theta_{\max}(\phi)$ defines the "perimeter" of the cylindrical source of particles and

$$\cos[\beta(\theta, \phi)] = \sqrt{\cos^2\theta + 1 - (R_1/R_2)^2 \sin^2\theta \sin^2\phi}.$$

Figure 8 shows the dependence of particle distribution on polar angle plotted for several values of azimuthal angle. The particle distribution is anisotropic in respect to the azimuthal angle. If the relaxation mechanisms are not strong enough this may result in an anisotropic surface structure.

B. Simulation of deposition

TiC/a-C nanocomposite films were grown on Si wafer by p-dc magnetron sputtering of graphite targets for various deposition times varied from 7.5 to 90 min at 100 kHz. Furthermore, after a deposition time of 90 min at 100 kHz, the deposition was continued for 30 to 180 min at 350 kHz. Two

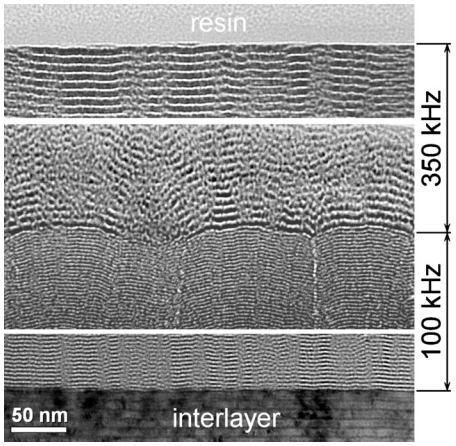

FIG. 9. Cross-sectional TEM micrograph of the TiC/a-C film $100C_{0.55}Ti\text{-}350C_{0.35}Ti$. The evolution of the structure clearly reveals that the roughness developed during 100 kHz p-dc sputtering was smoothened out by the subsequent 350 kHz p-dc sputtering.

sets of such depositions were carried out at a current of 0.35 and 0.55 Amp to the Ti-target. The detailed setup and deposition conditions have been described elsewhere.[14] Cross-sectional transmission electron microscopy) was performed to reveal the microstructural evolution during growth of the film along the thickness direction (Fig. 9). It is interesting to note that the surface roughness of the layers deposited at 100 kHz p-dc frequency experiences continuous roughening and those of 350 kHz p-dc sputtered layers exhibit rapid smoothing instead.

In this section, we compare the model predictions with the experimental data. Equations (7) and (25) are used to find the flux in each point of the surface. The initial surface profile is taken from an AFM scan of TiCr interlayer. To avoid contribution of deep narrow holes to rms roughness the AFM measurements are simulated with a parabolic tip ($r \sim 10$ nm). The input parameters for deposition simulation are listed in Table I. The configuration of the deposition system and the film growth rate correspond to the experiments.

The results of the calculations with the found angular distribution of "cylindrical magnetron" are shown in Figs. 10 and 11. Depositions with 100 kHz p-dc sputtering were simulated (labeled as 100 kHz in the figures) up to 1.5 h and then the simulations were continued by increasing the diffusion coefficients D_2 and D_4 to describe the higher flux of Ar^+ ions drawn to the substrate during 350 kHz p-dc sputtering. It should be mentioned that the effects of frequency and

TABLE I. Parameters used for deposition simulation during 100 and 350 kHz p-dc sputtering.

p-dc frequency	100 kHz	350 kHz
Growth rate, G, nm/s	0.13	0.05
Deposition noise, D, nm^4/s	1×10^{-3}	4×10^{-4}
Diffusion coefficients, D_2, nm^2/s	0.05	2
Diffusion coefficients, D_4, nm^4/s	0.5	1
System geometry, mm	$L=70$, $R_1=105$, $R_2=185$	
Sample size, nm (512×512 points)	2000	
Sputtering yield	$Y(\beta)\propto\cos^3\beta$	

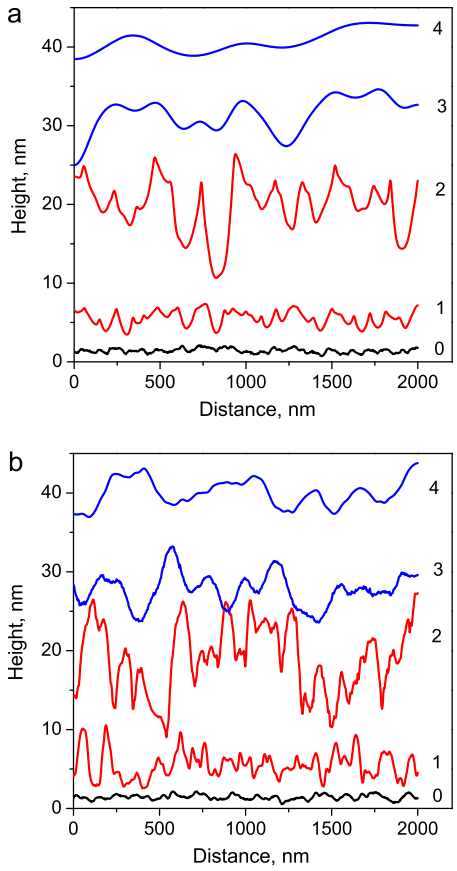

FIG. 10. (Color online) Evolution of the film surface profile. The sections $x=$const are taken from the central part of the simulation area (a) and the experimental AFM data (b). Profiles are shifted along the vertical axis by arbitrary values to make the roughness evolution clear. Labels have the following meaning: 0 denotes the initial profiles; 1 and 2 refer to deposition at 100 kHz for 0.5 and 1.5 h; and 3 and 4 refer to deposition at 350 kHz for additional 0.5 h and 1.5 h, respectively.

other parameters of p-dc sputtering on the deposition process and microstructure of TiC/a-C nanocomposite coatings were studied in details in Ref. 11. Time-averaged mass spectrometry measurements at the substrate position have revealed that pulsing the magnetron current leads to the generation of a significant fraction of middle and high energy Ar^+ ions onto the growing films. For example, during the sputtering of Ti-target at the same applied current, the energy distribution

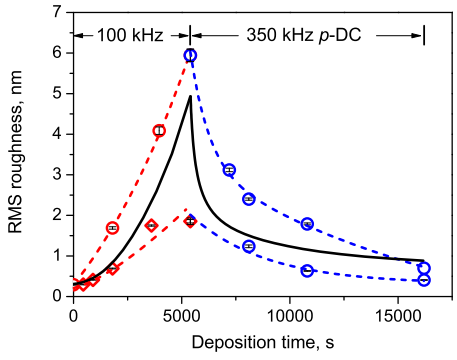

FIG. 11. (Color online) Surface rms roughness of TiC/a-C films as a function of deposition time. Solid line corresponds to simulations described in this section. Data points refer to two sets of depositions carried out at a current of 0.35 and 0.55 A to the Ti-target (for details see Ref. 14).

of impinging Ar^+ ions ends up at 20 eV with dc sputtering and at 90 eV, 140 eV, 180 eV, 205 eV, and 225 eV with p-dc sputtering of frequency 100 kHz, 200 kHz, 250 kHz, 300 kHz, and 350 kHz, respectively. As a consequence, the energy flux or intensity of concurrent ion impingement is enhanced from dc to 350 kHz p-dc sputtering by two orders of magnitude in sputtering Ti targets and almost three orders of magnitude in sputtering graphite targets, respectively.[11] It is considered that the enhanced concurrent impingement by Ar^+ ions of a wide energy distribution leads to a considerable increase in atomic mobility along the surface, which is reflected by the increase in diffusion coefficients in our simulation. The calculation of the explicit dependence of diffusion coefficients on p-dc frequency is beyond the scope of the present paper. Nevertheless, an approximate formula describing dependence of D_2 on the energy distribution of Ar^+ ions can be found in Ref. 13.

Figure 10 shows that the shadowing effect leads to amplification of initial large scale roughness during 100 kHz p-dc sputtering with a high deposition rate. At the same time small-scale features disappear due to the diffusion along the film surface. With increasing the diffusion coefficients D_2 and D_4 the surface becomes smoother; and only large scale hills remain, the size of which is comparable with the dimension of the simulation area. At the chosen diffusion parameters the anisotropy of the angular distribution (Fig. 8) did not resulted in noticeable anisotropy of the film surface. In Fig. 11 the simulation results are compared with the rms roughness measured experimentally. The numerical calculations presented in this section clearly reveal the influence of the deposition conditions and the diffusion parameters on the transition to shadowing growth.

V. CONCLUSIONS

(1) The shadowing growth of a film in three spatial dimensions has been studied within the framework of nonlocal model based on a stochastic partial differential equation which contains the second- and fourth-order diffusion terms. Our main goal was to demonstrate the influence of angular distribution of depositing particles on the onset and development of shadowing growth. The phenomenological continuum model developed in this paper helps to identify critical variables and parameters of deposition processes.

(2) Both the diffusion due to ballistic effects (D_2) and the curvature-driven diffusion (D_4) controls the transition to the shadowing growth. The curvature-driven diffusion accelerates the coarsening of the surface structure.

(3) The critical film thickness for transition to the shadowing growth is inversely proportional to the mean growth rate.

(4) The angular distribution of depositing particles strongly influence the transient time to the shadowing growth. Particles depositing at oblique angles (with polar angles close to $\theta=90°$) initiate the shadowing growth. By selecting the angular distribution function of depositing particles the shadowing instability can be effectively suppressed.

(5) The transition from the roughening regime of film growth to the smoothening one observed experimentally was analyzed. The linear growth of roughness developed during 100 kHz p-dc deposition has been attributed to the geometrical shadowing effect. To demonstrate the validity of the shadowing growth model the film growth has been simulated with the realistic particle angular distribution constructed taking into account the cylindrical magnetron geometry. Simulation results are in a good agreement with the experimental data on 100 and 350 kHz p-dc deposition. The dramatic decrease in the surface roughness when the frequency is changed from 100 to 350 kHz is explained by a strong increase in atomic diffusivity along the surface because of increased Ar^+ ion flux to the substrate.

ACKNOWLEDGMENTS

This research was carried out under the Project No. MC7.06246 in the framework of the Strategic Research program of the Materials innovation institute M2i, Delft, The Netherlands. The authors acknowledge financial support from the M2i and the Foundation for Fundamental Research on Matter FOM-Utrecht, the Netherlands. The Netherlands Organization for Scientific Research NWO is acknowledged for awarding a visitor's grant to one of the authors (A.A.T.).

[1] *Fractal Concepts in Surface Growth*, edited by A. L. Barabasi and H. E. Stanley (Cambridge University Press, Cambridge, 1995).
[2] J. Krug, Adv. Phys. **46**, 139 (1997).
[3] B. N. J. Persson, O. Albohr, U. Tartaglino, A. I. Volokitin, and E. Tosatti, J. Phys.: Condens. Matter **17**, R1 (2005).
[4] M. Pelliccione and T.-M. Lu, *Evolution of Thin Film Morphology: Modeling and Simulations* (Springer-Verlag, New York, 2008).
[5] P. Meakin, *Fractals, Scaling, and Growth Far from Equilibrium* (Cambridge University Press, Cambridge, 1998).
[6] D. L. Smith, *Thin-Film Deposition: Principles and Practice* (McGraw-Hill, New York, 1995).
[7] Y.-P. Zhao, G.-C. Wang, and T.-M. Lu, *Characterization of Amorphous and Crystalline Rough Surface: Principles and Applications* (Academic, New York, 2001).
[8] J. Robertson, Mater. Sci. Eng. R **37**, 129 (2002).
[9] D. R. McKenzie, D. Muller, and B. A. Pailthorpe, Phys. Rev. Lett. **67**, 773 (1991).
[10] R. G. Lacerda, P. Hammer, F. L. Freire, Jr., F. Alvarez, and F. C. Marques, Diamond Relat. Mater. **9**, 796 (2000).
[11] Y. T. Pei, C. Q. Chen, K. P. Shaha, J. T. M. De Hosson, J. W. Bradley, S. A. Voronin, and M. Cada, Acta Mater. **56**, 696 (2008).
[12] Y. T. Pei, K. P. Shaha, C. Q. Chen, R. van der Hulst, A. A. Turkin, D. I. Vainshtein, and J. T. M. De Hosson, Acta Mater. **57**, 5156 (2009).
[13] A. Turkin, Y. T. Pei, K. P. Shaha, C. Q. Chen, D. I. Vainshtein, and J. T. M. De Hosson, J. Appl. Phys. **105**, 013523 (2009).
[14] K. P. Shaha, Y. T. Pei, C. Q. Chen, A. A. Turkin, D. I. Vainshtein, and J. Th. M. De Hosson, Appl. Phys. Lett. **95**, 223102 (2009).
[15] F. Family and T. Vicsek, J. Phys. A **18**, L75 (1985).
[16] R. P. U. Karunasiri, R. Bruinsma, and K. Rudnick, Phys. Rev. Lett. **62**, 788 (1989).
[17] G. S. Bales and A. Zangwill, Phys. Rev. Lett. **63**, 692 (1989).
[18] C. Roland and H. Guo, Phys. Rev. Lett. **66**, 2104 (1991).
[19] J. H. Yao, C. Roland, and H. Guo, Phys. Rev. A **45**, 3903 (1992).
[20] G. S. Bales and A. Zangwill, J. Vac. Sci. Technol. A **9**, 145 (1991).
[21] J. Krug and P. Meakin, Phys. Rev. E **47**, R17 (1993).
[22] T. H. Vo Thi, J.-L. Rouet, P. Brault, J.-M. Bauchire, S. Cordier, and C. Josserand, J. Phys. D: Appl. Phys. **41**, 022003 (2008).
[23] J. H. Yao and H. Guo, Phys. Rev. E **47**, 1007 (1993).
[24] J. T. Drotar, Y.-P. Zhao, T.-M. Lu, and G.-C. Wang, Phys. Rev. B **62**, 2118 (2000).

[25]S. F. Edwards and D. R. Wilkinson, Proc. R. Soc. London, Ser. A **381**, 17 (1982).
[26]J. T. Drotar, Y.-P. Zhao, T.-M. Lu, and G.-C. Wang, Phys. Rev. B **61**, 3012 (2000).
[27]M. Moseler, P. Gumbsch, C. Casiraghi, A. C. Ferrari, and J. Robertson, Science **309**, 1545 (2005).
[28]W. W. Mullins, J. Appl. Phys. **28**, 333 (1957).
[29]Y. T. Pei, A. A. Turkin, C. Q. Chen, K. P. Shaha, D. Vainshtein, and J. T. M. De Hosson, Appl. Phys. Lett. **96**, 151910 (2010).
[30]B. A. Sperling and J. R. Abelson, Appl. Phys. Lett. **85**, 3456 (2004).
[31]T. Karabacak, H. Guclu, and M. Yuksel, Phys. Rev. B **79**, 195418 (2009).
[32]M. Raible, S. J. Linz, and P. Hänggi, Phys. Rev. E **62**, 1691 (2000).
[33]A. Vickery, C. P. Jensen, F. E. Christensen, M. P. Steenstrup, and T. Schønfeldt, X-Ray Optics and Instrumentation **2008**, 792540 (2008).
[34]T. Ono, T. Kenmotsu, and T. Muramoto, in *Reactive Sputter Deposition*, Springer Series in Materials Science Vol. 109, edited by D. Depla and S. Mahieu, (Springer, Berlin, 2008), pp. 1–42.
[35]H. Gnaser, in *Sputtering by Particle Bombardment*, Topics Applied Physics Vol. 110, edited by R. Behrisch and W. Eckstein (Springer-Verlag, Berlin, 2007, pp. 231–328.
[36]Y. Yamamura, Radiat. Eff. **55**, 49 (1981).
[37]Y. Yamamura, T. Takiguchi, and M. Ishida, Radiat. Eff. Defects Solids **118**, 237 (1991).
[38]W. O. Hofer, in *Sputtering by Particle Bombardment III: Characteristics of Sputtered Particles, Technical Applications*, Topics in Appl. Physics Vol. 64, edited by R. Behrisch and K. Wittmaack (Springer-Verlag, New York, 1991), pp. 15–90.
[39]K. Rödelsperger and A. Scharmann, Z. Phys. B **28**, 37 (1977).